# The Relevance of Mean-State Critical Levels for the Intensification of Downslope Winds in a Coastal Mountainous Environment

Gert-Jan Duine,[a] Leila M.V. Carvalho,[a,b] Charles Jones,[a,b] Callum F. Thompson,[a] William O.J. Brown,[c] John Dumas,[d] David Gomberg,[d] Todd Hall,[d] and Ryan Kittell[d]

[a] *Earth Research Institute, University of California Santa Barbara, Santa Barbara, California*

[b] *Department of Geography, University of California Santa Barbara, Santa Barbara, California*

[c] *National Center for Atmospheric Research, Boulder, Colorado*

[d] *National Weather Service, Los Angeles and Oxnard, California*

*Corresponding author*: Gert-Jan Duine, duine@eri.ucsb.edu



**Early Online Release:** This preliminary version has been accepted for publication in *Weather and Forecasting*, may be fully cited, and has been assigned DOI 10.1175/WAF-D-24-0084.1. The final typeset copyedited article will replace the EOR at the above DOI when it is published.

ABSTRACT: In wildfire-prone coastal Santa Barbara, California, downslope winds observed on the southern slopes of the east-west oriented Santa Ynez Mountains are known as Sundowner winds (or Sundowners). One important feature of Sundowners is the remarkable spatial and temporal variability in lee slope jet characteristics. Besides the intensity of the flow approaching the mountain range, the acceleration of the lee slope jet can be influenced by reflected gravity waves associated with one or more of the following mechanisms: a self-induced critical level, an inversion close to mountaintop, and the presence of a mean-state critical level (MSCL). The relative contribution of these mechanisms to the enhancement of Sundowners is yet unknown. This study uses 32-yr simulations (hourly, 1-km grid spacing) complemented with observations collected during the Sundowner Winds Experiment (SWEX) to better quantify the relative contribution of these mechanisms and to quantify the importance of MSCLs. We show that when an MSCL is present below 5 km, less atmospheric forcing is necessary to attain similar lee-slope jet strengths compared to when MSCLs are absent or above 5 km. This was evidenced from simulations and verified with observations. Although MSCLs during Sundowners occur year-round, their relative frequency increases in summer, when temperatures are high and fuels are dry, enhancing wildfire risk. Properly identifying these processes contributes to improved understanding and predictability of Sundowners and many other hazardous downslope windstorms in coastal environments.





Accepted for publication in *Weather and Forecasting*. DOI 10.1175/WAF-D-24-0084.1.

SIGNIFICANCE STATEMENT: Wildfires in coastal Santa Barbara, Southern California, are among the most disruptive hazards, and are influenced by strong winds that accelerate down the southern slopes of the Santa Ynez Mountain range. These winds are locally known as Sundowner winds, due to their appearance around sunset. Our goal is to understand how different atmospheric situations influence the surface winds at the south-facing slopes of the mountain range. We find that, when the atmosphere north of this mountain range contains a wind reversal (i.e., northerly winds turning southerly aloft), weaker winds below this reversal will induce winds on the south-facing slope that are stronger than with similar upstream winds without a reversal. Our findings are relevant to improve forecasting of Sundowner winds.

## 1. Introduction

Downslope windstorms occur all across the globe where air flow interacts with mountain barriers (Abatzoglou et al. 2021). Despite variability in mountain ranges, theory and observations of downslope windstorms have demonstrated that these events are associated with at least one of the following ingredients: 1) a strongly stably stratified layer close to mountaintop level below a layer of lower stability (Durran 1986); 2) a large-amplitude wave that breaks, thereby self-inducing a critical level (Peltier and Clark 1979); or 3) the presence of a critical level in the mean flow (Tomine 1984; Durran and Klemp 1987; Smith 2018). Although many studies have addressed the importance of these ingredients from case studies (Brinkmann 1974; Nance and Colman 2000; Grubišić et al. 2008; Koletsis et al. 2009), or idealized, theoretical and modeling studies (Durran and Klemp 1987; Miller and Durran 1991; Sheridan and Vosper 2006; Tollinger et al. 2019), the influence of the mean-state critical level (MSCL), typically defined as the level where cross-barrier winds reach zero, on the resultant lee slope flow is understudied.

Several studies have highlighted the relevance of MSCLs for the development of downslope windstorms. Using idealized simulations, Bacmeister and Pierrehumbert (1988) concluded that MSCLs affect gravity wave response for a wide range of non-dimensional critical levels. Colman and Dierking (1992) suggested that MSCLs must be present between 3.0-5.5 km above mean sea-level (MSL) for Taku winds in southeast Alaska to occur (the mountain range is around 1.2 km MSL), in addition to favorable strong cross-barrier flow and an inversion at or just above mountaintop (1.5-2.0 km MSL). Koletsis et al. (2009) examined a downslope windstorm case in





Accepted for publication in *Weather and Forecasting*. DOI 10.1175/WAF-D-24-0084.1.

Greece and found that MSCL was one of the main ingredients for its development. Moreover, for a variety of windstorms ranging from Alaska to the Rockies, gust forecasts based on a regional model were better captured during situations under MSCL presence, according to Nance and Colman (2000). Similarly, Metz and Durran (2023) suggested that the predictability of Santa Ana winds was improved under MSCL presence.

The east-west oriented Santa Ynez Mountains (SYM) represent an extensive barrier in coastal Santa Barbara, California. Occasionally, strong northerly winds accelerate on the southern slopes of these mountains. These winds are known as 'Sundowners', a name tied to the typical late afternoon-to-early evening onset (Blier 1998; Cannon et al. 2017). They exhibit remarkable spatiotemporal variability along the southern slopes of the SYM (Carvalho et al. 2020; Jones et al. 2021; Zigner et al. 2021). Jones et al. (2021) identified, based on Empirical Orthogonal Function analysis, three Sundowner regimes: western Sundowners, typically associated with NNW wind direction and strong winds on the western portion of the SYM; eastern Sundowners, associated with NNE wind direction and strong winds on the eastern portion of the SYM; hybrid Sundowners with strong winds on both eastern and western portions of the SYM.

Several studies have proposed a few mechanisms to explain the Sundowner winds. The intensification of the lee slope winds in the SYM has been linked to mountain wave development (Smith et al. 2018; Carvalho et al. 2020, 2024; Jones et al. 2021) and self-induced critical levels (Cannon et al. 2017; Duine et al. 2019, 2021). Moreover, climatological studies based on downscaling simulations have suggested that MSCLs can be present during Sundowners (Smith et al. 2018; Jones et al. 2021), but their role in the intensification of the winds has yet to be understood.

Coastal Santa Barbara is in a wildfire-prone region in Southern California, where numerous fast-spreading wildfires that disrupted local communities have been driven by Sundowner winds (Cannon et al. 2017; Zigner et al. 2020, 2022; Murray et al. 2021). Some of these events appeared related to the presence of an MSCL, notably the Holiday fire in July 2018 (Duine et al. 2022), the Painted Cave fire in June 1990 (Cannon et al. 2017), the Sherpa fire in June 2016 (Zigner et al. 2020), and the Whittier fire in July 2017 (Duine et al. 2019).

The National Weather Service (LA-Oxnard office, NWS/LOX) is the official institution responsible for the forecasts and warnings of Sundowner winds, and associated fire weather conditions. Their weather outlook primarily focuses on the development of synoptic patterns that may favor





Accepted for publication in *Weather and Forecasting*. DOI 10.1175/WAF-D-24-0084.1.

local pressure gradients conducive to Sundowner winds (Ryan 1996; Jones et al. 2021). However, the greatest uncertainty in forecasting Sundowner intensity appears when cross-mountain winds are forecast under relatively weak pressure gradients, which may happen more frequently during summer. In these situations, it is possible that MSCLs become an important factor in accelerating downslope winds, and this mechanism needs to be properly examined.

The main goal of this study is to investigate the importance of MSCL in intensifying Sundowner winds near the surface, comparatively to conditions without MSCL. These issues are primarily investigated using a Sundowner climatology (Jones et al. 2021). This climatology spans 32 years (1987-2019) of Weather & Research Forecasting (WRF) downscaling simulations at 1 km grid spacing (Jones et al. 2021). Climatological analyses are performed to evaluate the MSCL frequency, typical elevation, seasonality, and synoptic conditions associated with and without MSCLs. The relevance of upstream stability profiles on resulting downslope winds is also examined. The Sundowner Winds Experiment (SWEX) (Carvalho et al. 2024) that extended from 1 April to 15 May 2022 offers a unique opportunity to evaluate our modeling results against observations as Sundowners occurred under the presence and absence of MSCLs during the campaign.

The paper is organized as follows. Section 2 discusses the study area, simulations, observations, and methodology on how to define MSCLs. Section 3 discusses the MSCL variability, their climatology, their influence on lee slope winds relative to upstream environments, the synoptic settings of these events, and the MSCLs that were experienced during the SWEX field campaign. Concluding remarks are given in Section 4.

## 2. Data and methods

### *a. Study area & data*

The study area is located in southern California, and comprises a mix of east-west oriented mountain ranges just north of the Pacific Ocean (Fig. 1). This study focuses on the western Sundowner regime, for two reasons: these events are more frequent (Jones et al. 2021) and the NNW winds are less influenced by the high elevations of the San Rafael Mountains and the narrow portions of the Santa Ynez Valley (SYV, see Fig. 1). This minimizes the effects of the upstream terrain and better isolates the influence of MSCLs on Sundowners (Duine et al. 2021). To investigate the lee slope jet behavior, we selected the Refugio (RHWC1) and Montecito (MTIC1)





Accepted for publication in *Weather and Forecasting*. DOI 10.1175/WAF-D-24-0084.1.

locations as winds at these sites exhibit distinct spatial and temporal patterns during Sundowner conditions (Duine et al. 2021; Jones et al. 2021; Zigner et al. 2021). For the upstream profiles, we selected the lowest point in the SYV directly north of RHWC1, which is close to the Santa Ynez airport (KIZA). KIZA was selected due to its relative open terrain upstream (i.e., north) of the SYM.

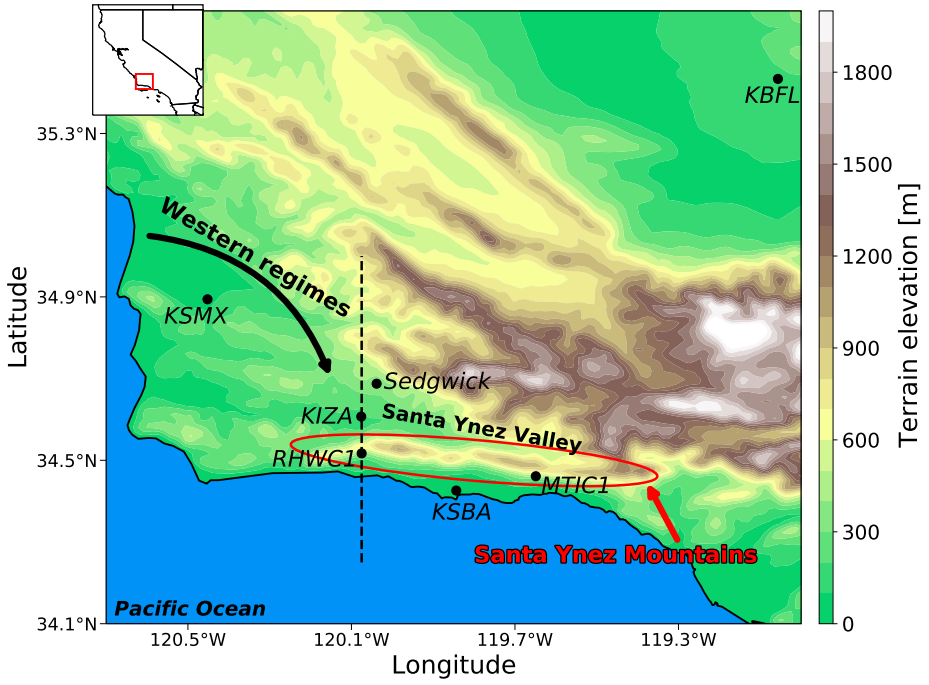


FIG. 1. Terrain elevation of the study area with relevant locations used in this study annotated. The dashed line highlights the longitude used for the cross-section composites, and intersects the upstream (KIZA) and downstream (RHWC1) locations. The air flow during western regime Sundowners approaches the Santa Ynez Mountain range from the northwest, as indicated by the black arrow. The inset map indicates the relative position of the study area in the state of California.

This study uses 32 years of Sundowner climatology from Jones et al. (2021). This data set was based on dynamically downscaled simulations with WRF version 4.0.1 (Skamarock and Klemp 2008), using ERA-Interim as initial and boundary conditions (Dee et al. 2011). The data spanned from July 1987 through June 2019 with hourly output. WRF was configured with four two-way nested grids to dynamically downscale from 27 km to 1 km using 55 vertical sigma levels and a model top at 50 hPa. Grid nudging was applied in the outermost domain on a 6-hr interval. Physical parameterizations included the Mellor-Yamada-Nakanishi-Niino level 2.5





Accepted for publication in *Weather and Forecasting*. DOI 10.1175/WAF-D-24-0084.1.

(MYNN) scheme (Nakanishi and Niino 2006) for the planetary boundary layer (PBL) – together with the recommended surface layer scheme – and the Noah MP land surface model (Niu et al. 2011). Other subgrid parameterizations used can be found in Duine et al. (2019), who investigated the model sensitivity at the surface in the study area.

Specifically, we separated the WRF climatology of western Sundowners into datasets with and without MSCLs to discern the influence of MSCL presence on the upstream environmental characteristics and downstream (lee slope) wind behavior. Note that Sundowner events are influenced by synoptic systems that may persist a few days, and occasionally, Sundowners are observed in two or more consecutive days (Jones et al. 2021). The persistence of days with Sundowners under the same MSCL environment was considered when performing statistical tests in this study (Wilks 2011). In this case, a sequence of multiple consecutive Sundowner days with the same MSCL environment was considered as one single event. Events that are separated by two or more days were considered independent in this study. Composites of synoptic analyses are performed with ERA5-reanalysis (Hersbach et al. 2020).

Observations of Sundowners during the SWEX field campaign (Carvalho et al. 2024) Intensive Operation Periods (IOPs) 4 and 9 with upstream MSCL and IOPs 3 and 10 without MSCL are discussed and compared. Additionally, we examined two Enhanced Observation Periods (EOPs), which focused on undisturbed conditions, that were associated with the presence of an MSCL. Radiosonde soundings (NSF NCAR – Earth Observing Laboratory 2022) released from the Sedgwick Reserve with the NSF NCAR Integrated Sounding System (NSF NCAR – Earth Observing Laboratory 1992–present; Parsons et al. 1994) were used for the MSCL analysis.

### *b. MSCL selection*

To define an MSCL, we adopted a similar method as in Durran and Klemp (1987). In this case, we assumed that an MSCL is defined at the elevation where the winds approaching a mountain range reach zero. Vertical profiles of horizontal winds upstream of the SYM were obtained at the center of the SYV (Fig. 1). Since the SYM is an east-west oriented mountain range, and RHWC1 is directly south of KIZA, approaching winds were defined as negative meridional wind component (V-component). An MSCL was considered present if the V-component was negative at SYM ridge level and reached zero at some elevation aloft (Fig. 2). The elevation of the MSCL was determined





Accepted for publication in *Weather and Forecasting*. DOI 10.1175/WAF-D-24-0084.1.

by linear interpolation. Profiles with only negative values for V-component were considered absent MSCLs ($MSCL_{none}$). Profiles with positive values (i.e., southerly winds) for V-component at the ridge level were classified as "other", and not considered in this study.

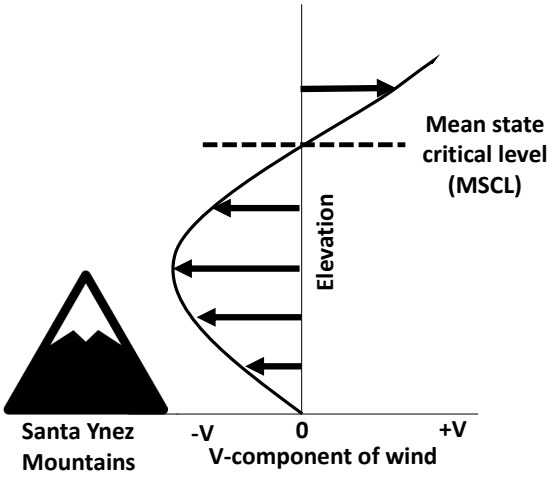


FIG. 2. Conceptual diagram of mean-state critical level (MSCL, dashed line) in the profile of winds upstream of a mountain range.

The data were separated into vertical profiles at KIZA that had: 1) MSCL presence below 5 km MSL ($MSCL_{<5km}$); 2) MSCL presence above 5 km MSL ($MSCL_{>5km}$); 3) absence of MSCL ($MSCL_{none}$). The 5-km threshold was chosen because the strong winds that are often observed at higher elevations in the troposphere unlikely contribute to mountain wave formation in relatively shallow mountain ranges (Colman and Dierking 1992; Nance and Colman 2000). Additionally, the 5 km threshold was used to retain abundant data while keeping the MSCL low enough to investigate a potential effect of MSCL presence on the lee slope wind behavior.

*c. Up- and downstream environment*

The importance of up- and downstream environment for the relevance of lee slope wind strength was determined by comparing composites of the MSCL and $MSCL_{none}$-environments, air mass properties up- and downstream of the SYM (Table 1), and individual profiles of winds across the SYM.




Accepted for publication in *Weather and Forecasting*. DOI 10.1175/WAF-D-24-0084.1.

The SYM upstream environment (i.e., winds and stability of the air mass) was evaluated above KIZA (Fig. 1). Upstream winds were diagnosed using the most negative value of the V-component below 5 km MSL ($V_{minUpstr}$), hence the same level to enhance comparability among the different MSCL profiles. Additionally, we examined V-components at ridge level ($V_{upstrRdgLvl}$), and 1000 m MSL ($V_{upstr1000}$), which were interpolated from model grid cells above and below these levels. The upstream stability was evaluated across ridge level by computing the Brunt-Väisälä frequency $N_{rdgLvl}$ using the model levels above and below model ridge level. The ridge level was determined as the highest point in the SYM along a north-south cross-section passing across KIZA. This elevation corresponds to 678.2 m MSL, or 489.2 m above ground level in the SYV at KIZA. The maximum value of $N$ ($N_{max}$) was diagnosed in these profiles below 3 km above ground level.

The influence of MSCL on lee-slope jet characteristics was assessed above RHWC1, which is roughly at mid-slopes of the SYM (Fig. 1). This location was selected for two reasons, it encounters strong downslope winds regularly and its elevation is high enough to be less affected by the shallow marine boundary layer (Duine et al. 2021; Zigner et al. 2021). We evaluated the lee slope wind strength at the surface ($V_{10Lee}$) and the most negative value of the V-component in the vertical profile ($V_{minLee}$) between the surface and about 3 km MSL.

TABLE 1. Summary of diagnostics used in this study.

| | Parameter | Variable | Units | Level | Range |
|---|---|---|---|---|---|
| Upstream | Level of mean-state | $MSCL$ | m | Variable | 0–10 km |
| | Minimum of $V$ | $V_{minUpstr}$ | m s$^{-1}$ | Variable | 0–5 km |
| | Cross-barrier winds | $V_{upstrRdgLvl}$ | m s$^{-1}$ | Ridge level | - |
| | | $V_{upstr1000}$ | m s$^{-1}$ | 1000 MSL | - |
| | Static stability | $N_{rdgLvl}$ | s$^{-1}$ | Ridge level | - |
| | Maximum static stability | $N_{max}$ | s$^{-1}$ | Variable | 0–3 km |
| Downstream | V-component 10 m | $V_{10Lee}$ | m s$^{-1}$ | 10 m | - |
| | Minimum of $V$ | $V_{minLee}$ | m | Variable | 0–3 km |

## 3. Results & Discussion

### *a. MSCL seasonal variability*

The monthly frequency of MSCLs during western regimes was examined from July 1987 to June 2019 at 21:00 PST (Fig. 3). This time of the day is after sunset in all seasons, when enhanced winds are expected to develop (Jones et al. 2021). Note that the majority of MSCLs were above





Accepted for publication in *Weather and Forecasting*. DOI 10.1175/WAF-D-24-0084.1.

10 km (Fig. 3). An MSCL above this level unlikely impacts downslope wind development (Metz and Durran 2023). The highest monthly frequency of $\text{MSCL}_{<5km}$ was in May, while the highest frequencies of MSCLs above 10 km and $\text{MSCL}_{none}$ were in April (Fig. 3). In a relative sense, $\text{MSCL}_{<5km}$ were less frequent than $\text{MSCL}_{>5km}$ throughout the year except in summer (Fig. 3). The latter reflects typical synoptic patterns affecting the region in this season (Jones et al. 2021). Synoptic systems are discussed in Section 3c.

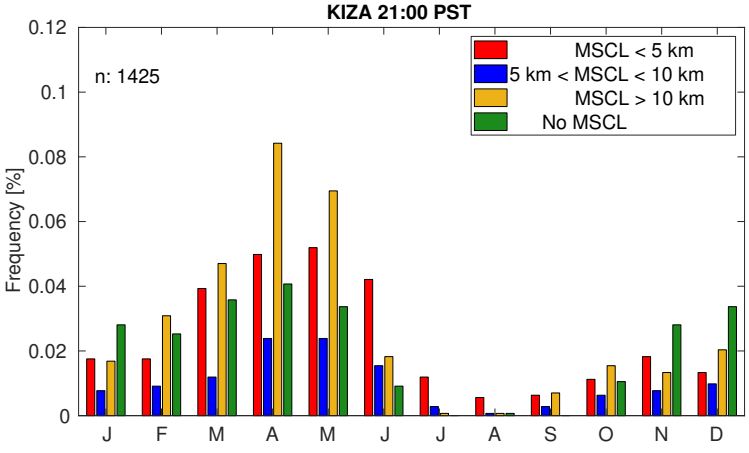


FIG. 3. Monthly frequency (%) of MSCL identified at 21:00 PST at KIZA and classified as western Sundowner. Period: July 1987 to June 2019 (total $n$ = 1425 events).

The seasonal variability of MSCLs is shown in Figure 4. MSCLs were evaluated below 10 km MSL, which is approximately the average tropopause height. Spring had the most MSCLs (285 days) and fall had the least (73 days). Seasonal distributions were relatively similar and skewed, with median values approximately between 3350 and 3750 m, modes of about 2.5 km and averages ranging from 4426.8 m in winter (Fig. 4a) to 4106.5 m MSL in fall (Fig. 4d). The highest (lowest) median MSCL is observed in DJF and JJA (SON). Interestingly, over 70% of spring and summer MSCLs occurred below 5 km (dashed lines in Fig. 4).

### *b. Up- and downstream environment*

To investigate differences in wind profiles and the importance of MSCL to the western Sundowners we computed composites of vertical cross sections of potential temperature, V-component and W-component along the Refugio longitude (see Fig. 1). To avoid redundancy, we focus the profile analysis in summer because of the relative importance of $\text{MSCLs}_{<5km}$ compared to other seasons





Accepted for publication in *Weather and Forecasting*. DOI 10.1175/WAF-D-24-0084.1.

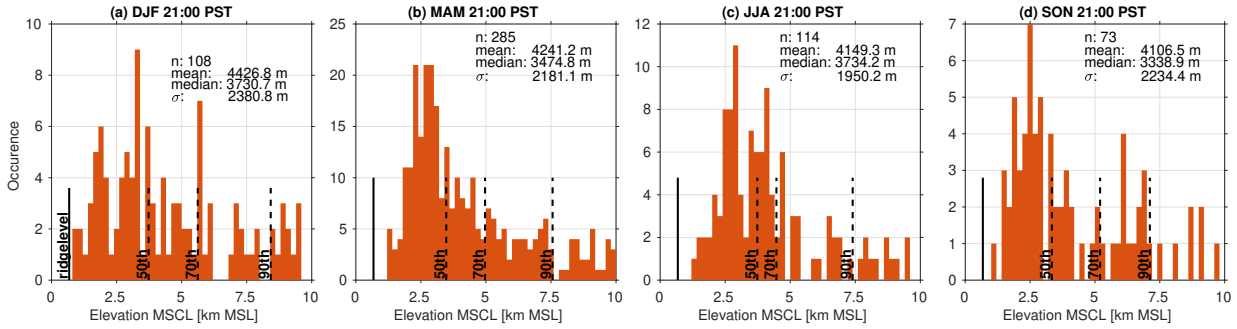


FIG. 4. (a-d) Seasonal histograms and statistics of MSCLs at 21:00 PST during western regimes. The profiles are evaluated up to 10 km MSL at KIZA (see Fig. 1). Vertical lines annotate ridge level (solid line), and the 50th, 70th, and 90th percentiles (dashed lines). Bin sizes are 200 m.

(Fig. 3). While Sundowners are rarer in summer, these events have greater impacts on wildfires. Figure 5 shows composites of the three different conditions during summer months. Other seasons are shown in Supplemental Figures S1-S3, and exhibit similar behavior. In summer, the majority of independent events (see Section 2a) were found with $\mathrm{MSCL}_{<5km}$ (59 cases, Fig. 5a,b), followed by $\mathrm{MSCL}_{>5km}$ (39 cases, Fig. 5c,d). Fewer cases were associated with $\mathrm{MSCL}_{none}$ (12 cases, Fig. 5e,f), in line with the monthly frequency (Fig. 3).

The average MSCL height for $\mathrm{MSCL}_{<5km}$-cases was around 3 km MSL (Fig. 5a). Below that level, winds approached the SYM at 1000 m MSL with cross-mountain (meridional) component of about –8 m s$^{-1}$ (Table 2). Note that a distinct layer of strong stratification is found in the SYV around ridge level ($N$=0.024 s$^{-1}$), topped by a layer with relatively weak stratification ($N$=0.012 s$^{-1}$). After crossing the SYM range, winds accelerated down the slope to average values exceeding –10 m s$^{-1}$ at RHWC1 (Table 2). Composites of the W-component reveal how gravity waves were constrained by the MSCL (Fig. 5b). Average vertical velocities above the lee (i.e., southern) slopes at RHWC1 reached –3.7 m s$^{-1}$ (Table 2). Further south on the foothills, composites suggest the presence of a hydraulic jump indicated by the positive W-component (Fig. 5b).

For the $\mathrm{MSCL}_{>5km}$-cases upstream of the SYM range, meridional winds weakened from –11 m s$^{-1}$ to less than –6 m s$^{-1}$ at 4 km MSL, highlighting backward shear (Fig. 5c). Backward shear is relevant to enhance mountain wave formation and lee slope wind acceleration (Fovell et al. 2022). Additionally, on the lee side of the SYM between 2000-3000 m MSL, we find a layer of weaker winds indicating that these cases were associated with wave breaking and the presence





Accepted for publication in *Weather and Forecasting*. DOI 10.1175/WAF-D-24-0084.1.

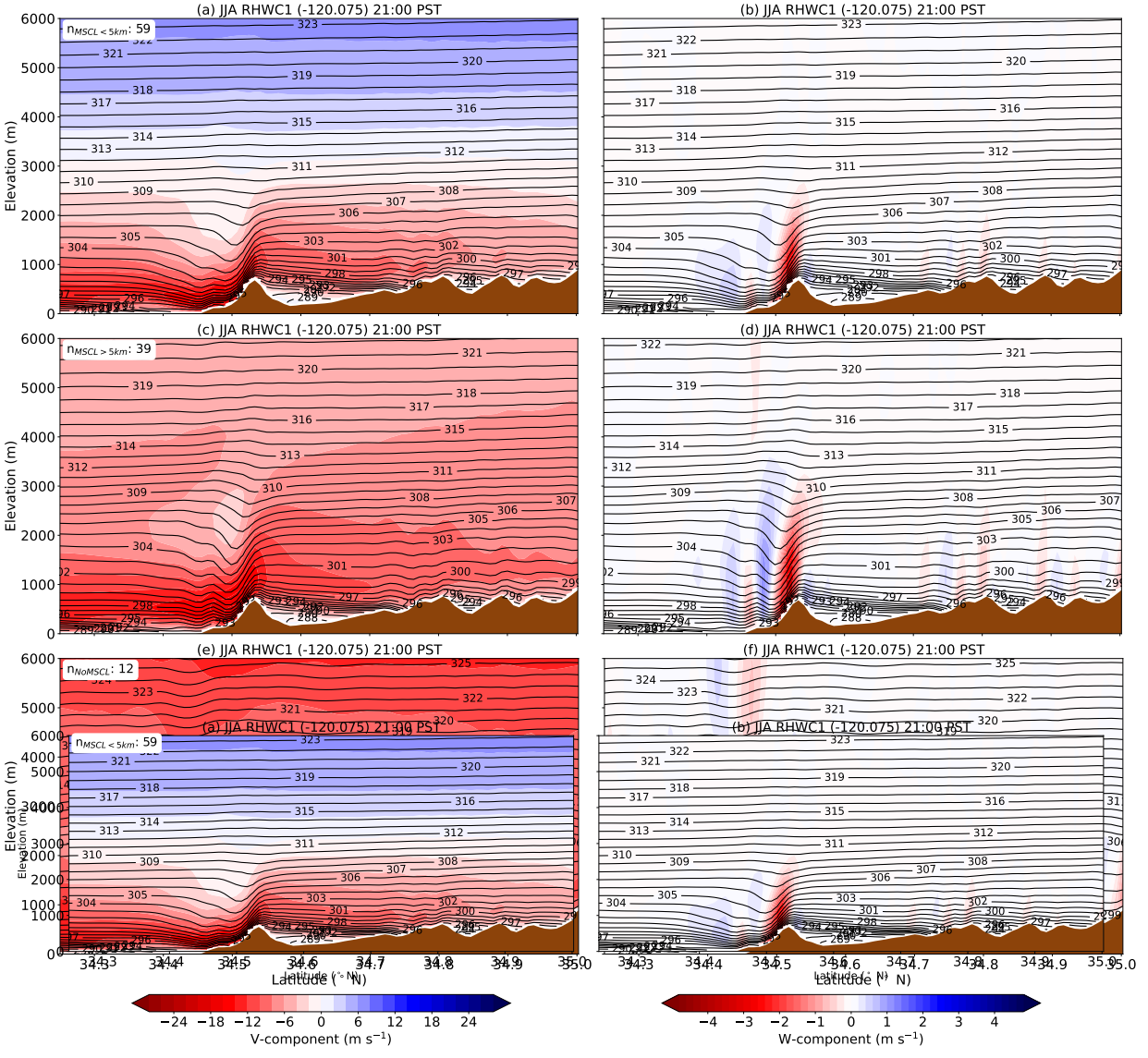


FIG. 5. Composite of vertical cross sections during summer months at 21:00 for (a,b) MSCL$_{<5km}$, (c,d) MSCL$_{>5km}$ and absent MSCLs, (a,c,d) meridional winds (colors) and $\theta$ (lines), and (b,d,f) for W-component (colors) and $\theta$ (lines) for RHWC1 cross-section (see Fig. 1 for location).

of a self-induced critical layer, as discussed in Cannon et al. (2017). Gravity waves reflected below the self-induced critical layer, as shown by the W-component (Fig. 5d). Despite the higher values of $V_{rdgLvl}$ compared to MSCL$_{<5km}$, the average lee slope winds at the surface were comparable (–10.0 m s$^{-1}$, Table 2). Vertical velocities reached around –3.7 m s$^{-1}$, similar to the MSCL$_{<5km}$. A





Accepted for publication in *Weather and Forecasting*. DOI 10.1175/WAF-D-24-0084.1.

TABLE 2. Summary of averages and standard deviation (in brackets) of variables for environments with $MSCL_{<5km}$, $MSCL_{>5km}$, and $MSCL_{none}$, separated by season. Profiles were evaluated upstream of the SYM (KIZA), and mid-slopes of the SYM (RHWC1). Averages are based on 32-yrs data western regimes at 21:00 PST. Histograms for JJA are shown in Supplemental Material Figure S4.

| | DJF | | | MAM | | |
|---|---|---|---|---|---|---|
| | $MSCL_{<5km}$ | $MSCL_{>5km}$ | No MSCL | $MSCL_{<5km}$ | $MSCL_{>5km}$ | No MSCL |
| $V_{upstrRdgLvl}$ [m s$^{-1}$] | –5.6 (4.0) | –8.2 (3.2) | –6.3 (2.7) | –4.6 (2.8) | –6.8 (3.2) | –5.3 (2.6) |
| $V_{upstr1000}$ [m s$^{-1}$] | –6.8 (4.7) | –10.5 (3.6) | –9.7 (3.2) | –7.3 (2.6) | –10.3 (3.0) | –10.6 (2.9) |
| $V_{minUpstr}$ [m s$^{-1}$] | –7.9 (4.3) | –12.8 (4.7) | –13.5 (4.7) | –8.2 (2.6) | –12.1 (3.8) | –13.0 (3.7) |
| $V_{10Lee}$ [m s$^{-1}$] | –6.5 (7.3) | –6.9 (2.0) | –7.1 (1.7) | –9.2 (2.2) | –8.7 (1.9) | –8.9 (1.6) |
| $V_{minLee}$ [m s$^{-1}$] | –13.1 (5.5) | –16.4 (3.8) | –15.5 (3.7) | –15.8 (3.6) | –17.6 (2.9) | –17.4 (2.5) |
| stability $N_{rdgLvl}$ [s$^{-1}$] | 0.011(0.005) | 0.011(0.005) | 0.015(0.005) | 0.018(0.007) | 0.017(0.007) | 0.020(0.004) |
| ratio $V_{10Lee}/V_{upstr1000}$ [%] | 0.0 | –34.3 | –26.8 | +26.0 | –15.5 | –16.0 |
| ratio $V_{minLee}/V_{minUpstr}$ [%] | +65.8 | +28.1 | +14.8 | +92.7 | +45.4 | +33.8 |
| | JJA | | | SON | | |
| | $MSCL_{<5km}$ | $MSCL_{>5km}$ | No MSCL | $MSCL_{<5km}$ | $MSCL_{>5km}$ | No MSCL |
| $V_{upstrRdgLvl}$ [m s$^{-1}$] | –3.9 (2.6) | –4.7 (2.5) | –4.0 (2.3) | –3.8 (2.6) | –7.9 (3.0) | –6.7 (3.2) |
| $V_{upstr1000}$ [m s$^{-1}$] | –8.6 (2.4) | –10.4 (2.0) | –11.8 (2.6) | –6.6 (2.5) | –10.1 (3.3) | –10.2 (3.7) |
| $V_{minUpstr}$ [m s$^{-1}$] | –9.5 (2.1) | –11.5 (2.3) | –13.0 (3.7) | –7.6 (2.7) | –12.1 (3.7) | –14.2 (5.4) |
| $V_{10Lee}$ [m s$^{-1}$] | –10.5 (1.1) | –10.0 (1.4) | –9.9 (1.1) | –8.1 (2.7) | –8.4 (1.8) | –6.8 (2.5) |
| $V_{minLee}$ [m s$^{-1}$] | –17.6 (1.9) | –18.0 (1.9) | –18.6 (2.1) | –13.9 (4.0) | –17.6 (2.9) | –15.7 (4.4) |
| stability $N_{rdgLvl}$ [s$^{-1}$] | 0.024(0.007) | 0.024(0.006) | 0.026(0.004) | 0.017(0.007) | 0.014(0.006) | 0.014(0.005) |
| $(V_{10Lee}-V_{upstr1000})/V_{upstr1000}$ [%] | +22.1 | –4.0 | –16.1 | +22.7 | –16.8 | –33.3 |
| $(V_{minLee}-V_{minUpstr})/V_{minUpstr}$ [%] | +85.2 | +56.5 | +43.1 | +82.9 | +45.4 | +10.6 |

stratified layer at ridge level upstream of the SYM was also apparent during $MSCL_{>5km}$, similarly to $MSCL_{<5km}$, also evidenced by $N_{rdgLvl}$ (Table 2).

Independent $MSCL_{none}$ events were observed in only 12 cases during summer (Fig. 5e,f). In these cases, we find northerly winds throughout the vertical profile upstream of the SYM. The average V-component at 1000 m MSL (in the SYV) was the strongest among all cases (–11.8 m s$^{-1}$, see Table 2). Even though the winds accelerated on the southern slopes (Fig. 5c), the average V-component on the lee slopes was similar to other cases (–9.9 m s$^{-1}$, Table 2). Among the relevant mechanisms responsible for the lee-slope jet acceleration is the formation of a self-induced critical layer above the lee slopes, as shown in Cannon et al. (2017). During $MSCL_{none}$, both mountain wave and hydraulic jump were present, and gravity waves propagated upward (Fig. 5f) due to the absence of MSCL, and/or the presence of forward shear. Note that the upward propagation of gravity waves was stronger in other seasons during $MSCL_{none}$ (Fig. S1-S3).





Accepted for publication in *Weather and Forecasting*. DOI 10.1175/WAF-D-24-0084.1.

One way to quantify the impact of MSCL on lee slope winds is to calculate the relative difference between winds over the lee slopes and upstream for the respective environments. We expressed these relationships in two ways. First, we calculated the percent difference between $V_{10Lee}$ and $V_{upstr1000}$. For $\text{MSCL}_{<5km}$ during summer, the average $V_{10Lee}$ exceed 22.1% of $V_{upstr1000}$ (see Table 2). For $\text{MSCL}_{>5km}$ and $\text{MSCL}_{none}$, the relative difference was –4.0% and –16.1%, respectively, indicating that the average $V_{upstr1000}$ still exceeded the downslope winds. When the relationship is expressed as the percent difference between $V_{minLee}$ and $V_{minUpstr}$ (i.e., $(V_{minLee}–V_{minUpstr})/V_{minUpstr}$), larger ratios are found: 85.2% for $\text{MSCL}_{<5km}$, 56.5% for $\text{MSCL}_{>5km}$, and 43.1% for $\text{MSCL}_{none}$. Similar behavior occurred in other seasons (Table 2). Therefore, any combination of these metrics yields similar conclusions: stronger lee slope winds require less upstream dynamic forcing when an MSCL is present.

Besides upstream winds, lee slope wind acceleration is also affected by static stability $N$. We measured $N$ at ridge level upstream of the SYM at KIZA (see Section 2c). Values of $N$ exceeding 0.02 $s^{-1}$ promote the inversion effect, while a typical value for static stability averaged across the troposphere is 0.01 $s^{-1}$ (Durran 1986). In summer, we found average values for $N_{rdgLvl}$ of around 0.024 $s^{-1}$ for cases with MSCL and 0.026 $s^{-1}$ for $\text{MSCL}_{none}$ (Table 2). In other seasons, $N_{rdgLvl}$ was equal or below 0.02 $s^{-1}$ (see Table 2). We also examined the existence of a linear correlation between $N_{max}$ and the value of $V_{10Lee}$ in all seasons and for all MSCL categories (Supplemental Table S1 and Figure S5). During JJA, statistically significant correlations (t-test at 0.05 significance level) were observed for $\text{MSCL}_{>5km}$ (r=–0.46). However, correlations increased during SON and were statistically significant for all MSCL categories (see Table S1). Conversely, correlations decreased in DJF and were statistically significant only for $\text{MSCL}_{<5km}$ (r=-0.31). Smith et al. (2018) also found higher values of stability in summer compared to other seasons, but concluded that stability in the upstream environment is rather "incidental to sundowner occurrence". Our findings, which are based on seasonal averages, underline their conclusion.

The impact of MSCL on Sundowner behavior is further examined by comparing differences between $\text{MSCL}_{<5km}$ and $\text{MSCL}_{none}$-composites of V-component in Figure 6. Note that differences were very similar in all seasons, with weaker winds (blue color) extending from the SYM ridge level to mid-troposphere during $\text{MSCL}_{<5km}$ compared to $\text{MSCL}_{none}$-cases. The most striking difference was on the lee slopes of the SYM. Despite the weaker winds aloft, stronger winds were





Accepted for publication in *Weather and Forecasting*. DOI 10.1175/WAF-D-24-0084.1.

observed on the slope and foothills of western SYM during $\text{MSCL}_{<5km}$. While the enhancement in the V-component was observed in all seasons, summer exhibits the largest differences (Fig. 6c), followed by fall (Fig. 6d) and spring (Fig. 6b). Differences appeared less important during winter (Fig. 6a).

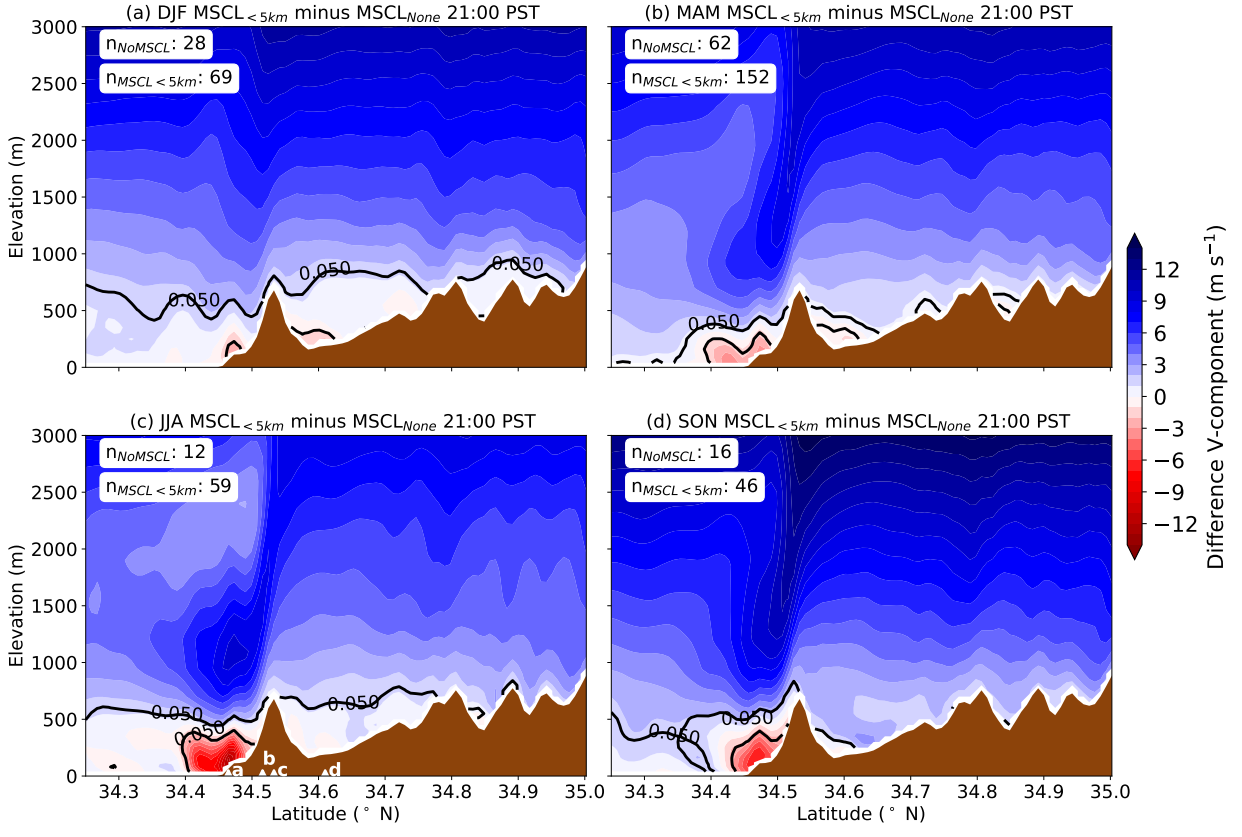


FIG. 6. Composite differences of V-component between MSCL for each season at 21:00 PST. Blue (red) colors indicate weaker (stronger) winds for $\text{MSCL}_{<5km}$ than for absent MSCLs. $n$ in the panels refers to the number of independent cases used for the composites. The contours highlight the boundaries of p=0.05, thus where the differences are statistically significant, according to a z-test (Wilks 2011). The annotated triangles in (c) indicate the locations shown in Figure 7.

To further investigate the role of MSCL in the intensification of Sundowners during summer, we examined composites of V-component (cross⊥mountain) wind profiles at four locations (21:00 PST) upstream (KIZA), mountaintop, halfway down the lee slopes and at the foothills of the SYM. The profiles of V-component upstream of the SYM at KIZA, showed weaker winds from ridge level upward for the $\text{MSCL}_{<5km}$, compared to $\text{MSCL}_{>5km}$ and $\text{MSCL}_{none}$-cases (Fig. 7d). The V-





Accepted for publication in *Weather and Forecasting*. DOI 10.1175/WAF-D-24-0084.1.

component peaked around the same elevation in all situations, although at slightly higher altitudes for the MSCL$_{none}$ (green). Note that the value of the V-component decreases more sharply with the elevation for MSCL$_{<5km}$ than for the other two cases.

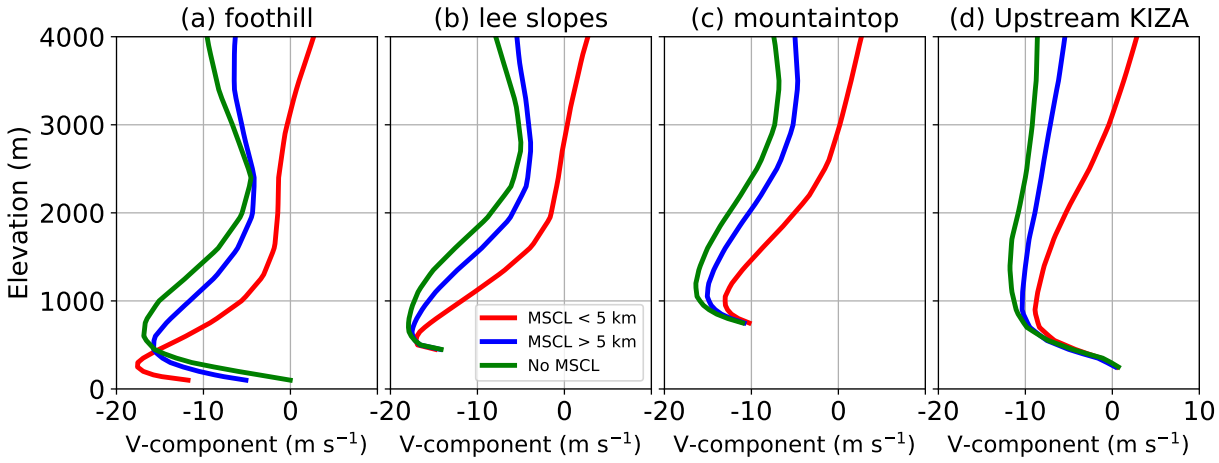


FIG. 7. Vertical profiles of V-component composites for MSCL$_{<5km}$ (red lines), MSCL$_{>5km}$ (blue) and MSCL$_{none}$ (green), at different locations for JJA. The locations of the profiles are marked by the triangles in Figure 6c. Legend in (b) applies to all panels.

The lee slope jet was well characterized on mountaintop, mid-slope and foothills of the SYM in all environments. However, a shallower lee slope jet appeared for MSCL$_{<5km}$ comparatively to MSCL$_{>5km}$ and MSCL$_{none}$. At the mountaintop (Fig. 7c), the peak of the V-component was weaker for MSCL$_{<5km}$ (around –13 m s$^{-1}$), compared to MSCL$_{>5km}$ (around –15 m s$^{-1}$) and MSCL$_{none}$ (around –16 m s$^{-1}$). Comparable values were found at the surface (approximately –10 m s$^{-1}$). The average height of the peak of MSCL$_{<5km}$ V-component was around 1000 m, slightly lower than the other two cases. At mid-slopes (Fig. 7b), the profiles were similar closer to the surface but differed at higher elevations, with the MSCL$_{<5km}$-cases showing that the jet peaks at similar strength (about –17 m s$^{-1}$), but is confined to lower elevations, compared to MSCL$_{<5km}$ and MSCL$_{none}$.

The largest differences among the profiles was found at the foothills (Fig. 7a). For MSCL$_{<5km}$-cases, the averaged profiles show a strong and shallow lee slope jet, whereas the MSCL$_{>5km}$ and MSCL$_{none}$-cases show less pronounced jets with weaker jet peaks at higher elevations. Remarkable differences were also found near the surface where average values for V-component during MSCL$_{<5km}$ were about –12 m s$^{-1}$, whereas during MSCL$_{>5km}$ and MSCL$_{none}$,





Accepted for publication in *Weather and Forecasting*. DOI 10.1175/WAF-D-24-0084.1.

values for V-component were around –5 m $s^{-1}$ and zero, respectively. This could indicate that there was more variability in the horizontal extent of lee slope jets during the $MSCL_{none}$ and $MSCL_{>5km}$-cases, than during $MSCL_{<5km}$-cases (see e.g. Figure S4h in supplemental material).

### *c. Synoptic conditions*

While lee-slope jet accelerations are a mesoscale phenomenon, the synoptic configuration plays a major role in setting up the environment conducive to MSCL presence. Here, we explore the differences in synoptic forcings by comparing composites of the mean-sea level pressure (MSLP), winds at 850 hPa, and geopotential height at 500 hPa during $MSCL_{<5km}$, $MSCL_{>5km}$ and $MSCL_{none}$ for JJA (Fig. 8). All three environments were observed with a northerly wind component at 850 hPa, approximately 1500 m MSL, about twice the terrain elevation of the SYM peak at RHWC1 (Fig. 8).

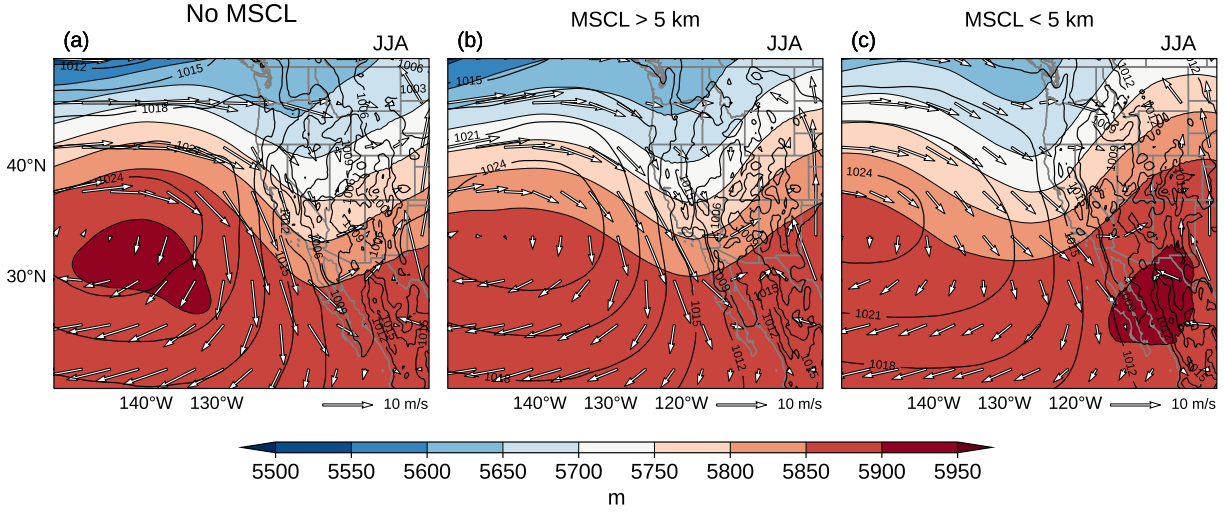


FIG. 8. Composites of geopotential height at 500 hPa (color, m), winds at 850 hPa (arrows), and sea-level pressure (contours, mbar) for (a) $MSCL_{none}$, (b) $MSCL_{>5km}$, and (c) $MSCL_{<5km}$ for summer (JJA) months. Data is from ERA5.

During $MSCL_{none}$, a pronounced ridge at 500 hPa, aligned with the center of an anticyclone at surface level, was located over Eastern Pacific at subtropical latitudes, whereas a trough was evident over west continental USA, with the trough axis centered over central Nevada (Fig. 8a). A similar ridge-trough pattern has been shown in the spring (March-May) climatology during western Sundowners by Jones et al. (2021). Although the ridge-trough pair still existed for $MSCL_{>5km}$ (Fig. 8b), the ridge axes over the subtropical eastern Pacific at 500 hPa was not aligned with





Accepted for publication in *Weather and Forecasting*. DOI 10.1175/WAF-D-24-0084.1.

the center of the Pacific anticyclone, which is consistent with the decreased ridge amplitude and the westward displacement of the trough. Notably, the trough axis was located over California, allowing flow aloft to be more zonal over Santa Barbara.

The most remarkable difference in patterns is shown in the composites of $\text{MSCL}_{<5km}$ (Fig. 8c). During summer, a shallow thermal low (less than 3500 m) typically develops over south-western USA and north-western Mexico (Rowson and Colucci 1992). The ascending air associated with this thermal low increases geopotential height in mid-levels of the atmosphere, as shown by the closed center with geopotential heights exceeding 5900 m over Baja California (Fig. 8c). Additionally, the ridge-trough pair over the subtropical eastern Pacific shifts westward, with the trough axis observed off the California coast. These combined features result in flow above Santa Barbara turning southwesterly with elevation, often below 500 hPa, thereby optimizing conditions conducive to $\text{MSCL}_{<5km}$. Notably, MSLP gradients around SBA were weaker for $\text{MSCL}_{<5km}$ than during $\text{MSCL}_{none}$. This synoptic settings for $\text{MSCL}_{<5km}$ reflect the situation described as a "severe or category 3 Sundowner" in Ryan (1996). Similar synoptic settings are observed in other seasons, except for the thermal low that is typically observed during summer (see Supplemental Material Figure S6).

These synoptic analyses demonstrated that Sundowners developing under MSCL presence required much weaker MSLP gradients to reach similar strength on the southern slopes of the SYM, comparatively to $\text{MSCL}_{none}$. These findings indicate that the accurate forecast of MSCLs (such as the development of a thermal low during summer), can be critical in forecasting strong Sundowner winds when pressure gradients do not exceed thresholds statistically associated with significant Sundowner events (e.g., Ryan (1996); Sukup (2013); Jones et al. (2021)).

### *d. MSCL during SWEX 2022*

SWEX was conducted from April 1 to May 15 2022, and aimed at improving understanding of mesoscale mechanisms related to Sundowner winds (Carvalho et al. 2024). A total of 10 IOPs were conducted under a variety of synoptic and mesoscale forcing, and 3 EOPs were conducted under weak synoptic forcing. Out of these 13 missions, two IOPs (4 and 9) and two EOPs (1 and 2) were carried out with the presence of MSCL below 5 km MSL. Table 3 summarizes mission dates, including details on the Sundowner regime and MSCL. We used the radiosonde observations from





Accepted for publication in *Weather and Forecasting*. DOI 10.1175/WAF-D-24-0084.1.

Sedgwick reserve at 21:00 PST for diagnosis of MSCL. Sedgwick reserve is located upstream of the SYM (see Fig. 1). A more complete description of the campaign can be found in the SWEX overview paper (Carvalho et al. 2024).

TABLE 3. Details on SWEX IOPs and EOPs for this study, including start dates, their specific Sundowner regime and the height of the MSCL. IOP/EOP duration was typically 24 hours. MSCLs were diagnosed by radiosonde soundings released from Sedgwick (see Fig. 1), the profiles are shown in Supplemental Figure S7.

| | IOP/EOP start [PST] | Regime | MSCL at 21:00 PST [m MSL] |
|---|---|---|---|
| IOP 03 | Apr. 13 09:00 | Western | $\text{MSCL}_{none}$ |
| IOP 04 | Apr. 18 09:00 | Western | 2433 |
| IOP 09 | May 10 09:00 | Western | 3818 |
| IOP 10 | May 12 09:00 | Hybrid | $\text{MSCL}_{none}$ |
| EOP 01 | Apr. 17 09:00 | – | 3623 |
| EOP 02 | Apr. 25 09:00 | – | 1385 |

We compared observed MSLP differences and lee slope winds during the IOP 4 associated with $\text{MSCL}_{<5km}$ with IOP 3 with $\text{MSCL}_{none}$, both were classified as western regime (Table 3). For the lee slope wind observations, we focused on RHWC1 station, as this location is roughly halfway along the lee slopes and relatively far away from coastal influences. Moreover, the strongest winds during IOP 4 were observed at RHWC1. The NWS/LOX utilizes MSLP differences between the Santa Maria (KSMX) and Santa Barbara (KSBA) airports and Bakersfield (KBFL) and KSBA (see Fig. 1 for their locations) as a metric for western and eastern Sundowner intensity, respectively (Ryan 1996; Carvalho et al. 2020; Duine et al. 2021; Jones et al. 2021). Therefore, to properly compare these cases, we compared IOPs 3 and 4 using RHWC1 and KSBA-KSMX MSLP difference.

Figure 9a,b compares the hourly observations of the V-component and gusts at RHWC1 (elevation 446.5 m MSL, Fig. 1), with the MSLP differences between KSBA and KSMX for all SWEX hourly observations (black dots). Data from IOPs 3 and 4 are highlighted with blue and red crosses, respectively. On average, slightly weaker MSLP-differences were observed during IOP 3 comparatively to IOP 4. In line with the results of the climatology from previous sections, we found that during the $\text{MSCL}_{<5km}$ of IOP 4, both more negative V-components (Fig. 9a) and stronger gusts (Fig. 9b) were observed, relatively to the $\text{MSCL}_{none}$ of IOP 3. IOP 4 MSCL was observed at 2433 m at 21:00 PST (Table 3 and Supplemental Figure S7a). Supplemental Figure S8 further compares vertical cross sections for IOPs 3 and 4.




Accepted for publication in *Weather and Forecasting*. DOI 10.1175/WAF-D-24-0084.1.

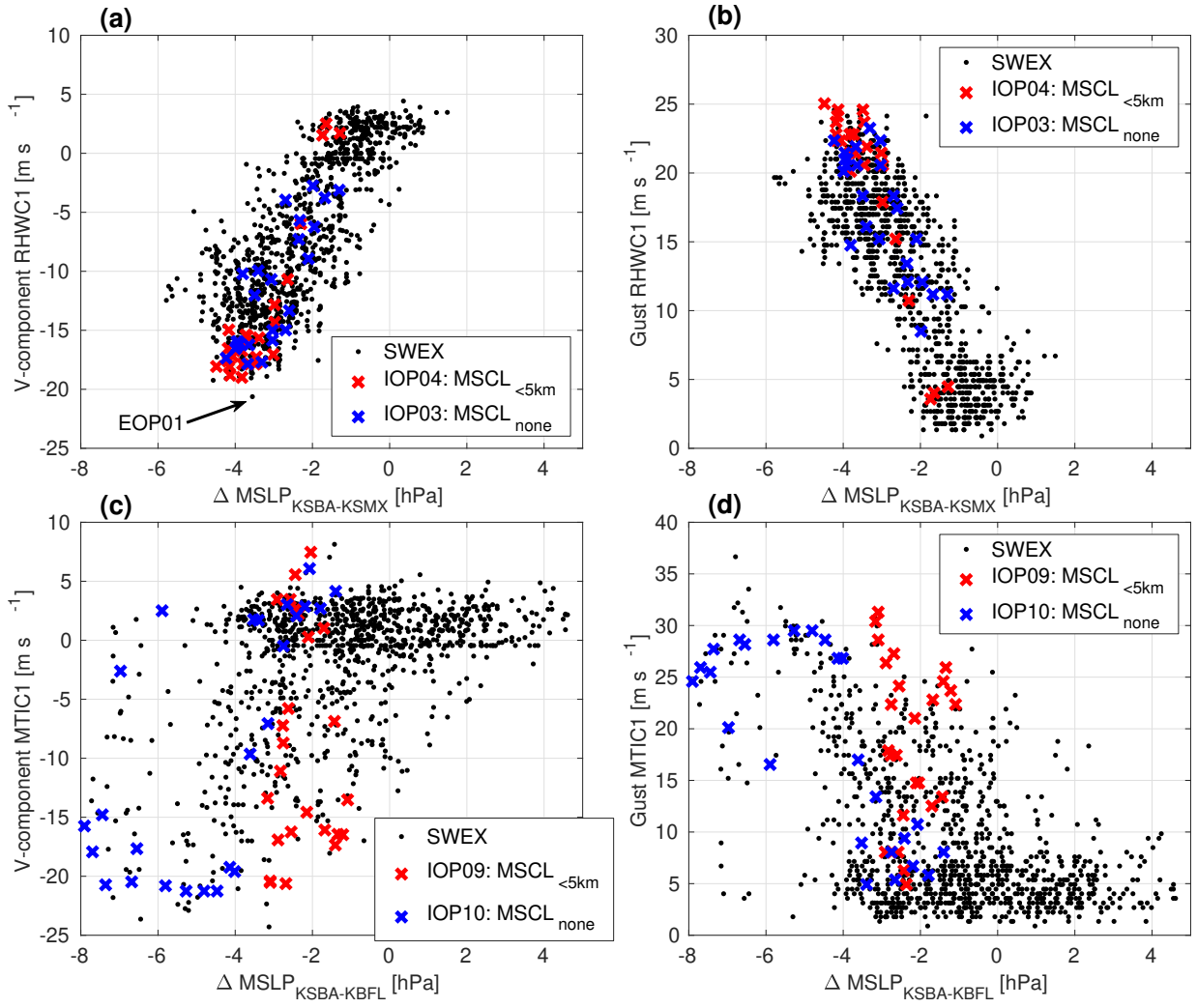


FIG. 9. Hourly observations of MSLP differences between KSBA and KSMX or KBFL compared to observed (a) V-component and (b) gusts at RHWC1, and (c) V-component and (d) gusts at MTIC1. Each plot shows all hourly observations during the SWEX period April 1 - May 15 2022 (black dots) and highlights the same observations but then for IOPs that were undergoing MSCL (IOPs 4 and 9, red crosses) and compared to MSCL (IOPs 3 and 10). The strongest wind at RHWC1 during SWEX is highlighted using an arrow in (a). The highlighted IOPs are 24 hours from start dates given in Table 3.

We found similar features during other IOPs and EOPs. For example, IOP 9, that occurred with an MSCL of 3818 m MSL at 21:00 PST, showed weaker tropospheric forcing than IOP 10, that occurred without MSCL (see Table 1 and Fig. 9c,d). Regardless, winds were similarly strong at MTIC1 during both IOPs. Note that for this comparison we used a different station (MTIC1) to





Accepted for publication in *Weather and Forecasting*. DOI 10.1175/WAF-D-24-0084.1.

evaluate lee slope winds, as this location observed the strongest winds during IOPs 9 and 10, and we compared this using the MSLP difference between KSBA and KBFL, a metric more representative for winds in eastern SYM (see Fig. 1). Moreover, the strongest wind (V-component of –20.6 m $s^{-1}$) of the full SWEX period at RHWC1 was recorded during EOP 1, even though EOPs primarily focused on weak synoptic forcing (see annotated arrow in Fig. 9a). Finally, the strongest winds that developed during EOP 2, reached –14.1 m $s^{-1}$ at RHWC1, thereby surpassing coastal wind advisory levels.

These IOP- and EOP-comparisons confirmed the results of the 32-yr climatology from an observational perspective. The cases provided evidence of the importance of MSCL for mountain waves and resulting lee-slope jet characteristics, indicating that MSCL presence can enhance winds on the slopes and foothills of the SYM. Our findings further underline that even under the weakest forcing, downslope winds may develop stronger than anticipated.

## 4. Conclusion

We have investigated the influence of mean-state critical levels (MSCLs) on the formation of downslope windstorms in coastal Santa Barbara, known as Sundowners. These strong downslope winds increase the potential for wildfire hazards due to their strength and association with low humidities and occasional high temperatures. Using a 32-yr WRF Sundowner wind climatology (1987-2019) at 1 km grid spacing, and observations collected during the SWEX field experiment (April 1 to May 15 2022), we demonstrated that weaker synoptic forcing and upstream winds may result in similar lee slope wind strength under MSCL presence.

For our investigation, we primarily focused on the western SYM during western Sundowner regimes. We found that MSCLs occur year-round, with similar elevations throughout the year, the majority below 5 km MSL. While Sundowners occur most frequently in spring, the relative importance of the MSCL peaks in summer, when synoptic forcings are generally weaker. Comparisons between up- and downstream environments with and without MSCLs, regardless of cross-barrier flow at different elevations and stability above and at ridge level, indicated that stronger lee slope winds were simulated when MSCLs were present, especially during $\mathrm{MSCL}_{<5km}$. Synoptic analyses indicated that $\mathrm{MSCL}_{<5km}$ are observed in all seasons when a ridge-trough pair is displaced westward over the Pacific with respect to their position during $\mathrm{MSCL}_{none}$. This synoptic set up





Accepted for publication in *Weather and Forecasting*. DOI 10.1175/WAF-D-24-0084.1.

favors southerly winds below mid-levels across Santa Barbara. In summer, the typical development of a shallow thermal low and topped by a mid-tropospheric ridge over Baja California, reinforce the southerly flow over southern California below 5 km.

During the SWEX campaign, two IOPs and two EOPs (out of a total of 13 missions) were conducted with $\text{MSCL}_{<5km}$. In particular, the strongest wind at RHWC1 (western SYM) for the SWEX period was reported during EOP1, during relatively weak pressure gradients. Comparisons between IOPs 3 and 4, and 9 and 10, respectively, revealed that stronger lee slope winds were observed in the presence of MSCL, despite similar upstream forcing between IOP 3 ($\text{MSCL}_{none}$) and IOP 4 ($\text{MSCL}_{<5km}$), and weaker forcing for IOP 9 ($\text{MSCL}_{<5km}$) compared to IOP 10 ($\text{MSCL}_{none}$).

These results show that incorporating metrics to evaluate MSCL presence and elevation can be helpful in forecasting strong downslope winds when cross-mountain winds are expected, even when MSLP gradients are relatively weak and may not exceed pre-established thresholds known to be associated with strong lee slope winds. Additionally, the differences between the cases ($\text{MSCL}_{<5km}$ vs. $\text{MSCL}_{none}$) were largest for summer. With generally weaker pressure gradients, the presence of an $\text{MSCL}_{<5km}$ may represent enhanced potential for destructive winds, high temperatures, low humidity and thus fast spreading wildfires, especially in California when dry summers may significantly decrease fuel moisture. Notably, Sundowner events associated with significant wildfires in coastal Santa Barbara during summer, such as the Painted Cave, Sherpa, Whittier, and Holiday fires, occurred in the presence of an MSCL.





Accepted for publication in *Weather and Forecasting*. DOI 10.1175/WAF-D-24-0084.1.

*Acknowledgments.* This research was supported by the Integrative and Collaborative Education and Research (ICER) program, from the National Science Foundation (NSF-ICER-1664173), the NSF-1921595 that supported the Sundowner Winds field EXperiment SWEX in Spring of 2022, and University of California Laboratory Fees Research Program (LFR-20-652467) 'Mitigating and Managing Extreme Wildfire Risk in California' project. Gert-Jan Duine was partially supported by the Gordon and Betty Moore Foundation through Grant GBMF11601 and NSF-AGS 2331728 (Understanding the Influence of Turbulent Processes on the Spatiotemporal Variability of Downslope Winds in Coastal Environments). We acknowledge high-performance computing support from the NSF NCAR Computational and Information Systems Laboratory using the Cheyenne supercomputer (https://doi.org/10.5065/D6RX99HX).

*Data availability statement.* The data for 32-yr simulations can be accessed by contacting Charles Jones (https://clivac.eri.ucsb.edu/clivac/Regional_Climate/index.html). The SWEX field experiment data, including radiosonde data, is freely available in the SWEX Field Catalog https://catalog.eol.ucar.edu/swex.

## References

Abatzoglou, J. T., B. J. Hatchett, P. Fox-Hughes, A. Gershunov, and N. J. Nauslar, 2021: Global climatology of synoptically-forced downslope winds. *Int. J. Clim.*, **41 (1)**, 31–50.

Bacmeister, J., and R. Pierrehumbert, 1988: On high-drag states of nonlinear stratified flow over an obstacle. *J. Atmos. Sci.*, **45 (1)**, 63–80.

Blier, W., 1998: The sundowner winds of Santa Barbara, California. *Weather Forecast.*, **13 (3)**, 702–716.

Brinkmann, W. A., 1974: Strong downslope winds at Boulder, Colorado. *Mon. Wea. Rev.*, **102 (8)**, 592–602.

Cannon, F., L. M. Carvalho, C. Jones, T. Hall, D. Gomberg, J. Dumas, and M. Jackson, 2017: WRF simulation of downslope wind events in coastal Santa Barbara County. *Atmos. Res.*, **191**, 57–73.





Accepted for publication in *Weather and Forecasting*. DOI 10.1175/WAF-D-24-0084.1.

Carvalho, L. M., and Coauthors, 2020: The Sundowner Winds Experiment (SWEX) Pilot Study: Understanding Downslope windstorms in the Santa Ynez Mountains, Santa Barbara, California. *Mon. Wea. Rev.*, **148 (4)**, 1519–1539.

Carvalho, L. M., and Coauthors, 2024: The Sundowner Winds Experiment (SWEX) in Santa Barbara, California: Advancing Understanding and Predictability of Downslope Windstorms in Coastal Environments. *B. Am. Meteorol. Soc.*, **105 (3)**, E532–E558.

Colman, B. R., and C. F. Dierking, 1992: The Taku wind of southeast Alaska: Its identification and prediction. *Weather Forecast.*, **7 (1)**, 49–64.

Dee, D. P., and Coauthors, 2011: The ERA-Interim reanalysis: Configuration and performance of the data assimilation system. *Q. J. Roy. Meteor. Soc.*, **137 (656)**, 553–597.

Duine, G.-J., L. M. Carvalho, and C. Jones, 2022: Mesoscale patterns associated with two distinct heatwave events in coastal Santa Barbara, California, and their impact on local fire risk conditions. *Weather and Climate Extremes*, **37**, 100 482.

Duine, G.-J., L. M. Carvalho, C. Jones, and K. Zigner, 2021: The Effect of Upstream Orography on the Onset of Sundowner Winds in Coastal Santa Barbara, CA. *J. Geophys. Res.-Atmos.*, **126 (8)**, e2020JD033 791.

Duine, G.-J., C. Jones, L. M. Carvalho, and R. G. Fovell, 2019: Simulating Sundowner Winds in Coastal Santa Barbara: Model Validation and Sensitivity. *Atmosphere*, **10 (3)**, 155.

Durran, D. R., 1986: Another look at downslope windstorms. Part I: The development of analogs to supercritical flow in an infinitely deep, continuously stratified fluid. *J. Atmos. Sci.*, **43 (21)**, 2527–2543.

Durran, D. R., and J. B. Klemp, 1987: Another look at downslope winds. Part II: Nonlinear amplification beneath wave-overturning layers. *J. Atmos. Sci.*, **44 (22)**, 3402–3412.

Fovell, R. G., M. J. Brewer, and R. J. Garmong, 2022: The December 2021 Marshall Fire: Predictability and Gust Forecasts from Operational Models. *Atmosphere*, **13 (5)**, 765.

Grubišić, V., and Coauthors, 2008: The Terrain-Induced Rotor Experiment: A field campaign overview including observational highlights. *B. Am. Meteorol. Soc.*, **89 (10)**, 1513–1534.





Accepted for publication in *Weather and Forecasting*. DOI 10.1175/WAF-D-24-0084.1.

Hersbach, H., and Coauthors, 2020: The ERA5 global reanalysis. *Q. J. Roy. Meteor. Soc.*, **146 (730)**, 1999–2049.

Jones, C., L. M. Carvalho, G.-J. Duine, and K. Zigner, 2021: Climatology of Sundowner winds in coastal Santa Barbara, California, based on 30 yr high resolution WRF downscaling. *Atmos. Res.*, **249**, 105 305.

Koletsis, I., K. Lagouvardos, V. Kotroni, and A. Bartzokas, 2009: Numerical study of a downslope windstorm in Northwestern Greece. *Atmos. Res.*, **94 (2)**, 178–193.

Metz, J. J., and D. R. Durran, 2023: Downslope Windstorm Forecasting: Easier with a Critical Level, but Still Challenging for High-Resolution Ensembles. *Weather Forecast.*, **38 (8)**, 1375 – 1390, https://doi.org/10.1175/WAF-D-22-0135.1.

Miller, P. P., and D. R. Durran, 1991: On the sensitivity of downslope windstorms to the asymmetry of the mountain profile. *J. Atmos. Sci.*, **48 (12)**, 1457–1473.

Murray, A. T., L. Carvalho, R. L. Church, C. Jones, D. Roberts, J. Xu, K. Zigner, and D. Nash, 2021: Coastal vulnerability under extreme weather. *Appl. Spat. Anal. Polic.*, **14 (3)**, 497–523.

Nakanishi, M., and H. Niino, 2006: An improved Mellor–Yamada level-3 model: Its numerical stability and application to a regional prediction of advection fog. *Bound.-Lay. Meteorol.*, **119 (2)**, 397–407.

Nance, L. B., and B. R. Colman, 2000: Evaluating the use of a nonlinear two-dimensional model in downslope windstorm forecasts. *Weather Forecast.*, **15 (6)**, 715–729.

Niu, G.-Y., and Coauthors, 2011: The community Noah land surface model with multiparameterization options (Noah-MP): 1. Model description and evaluation with local-scale measurements. *J. Geophys. Res.-Atmos.*, **116 (D12)**.

NSF NCAR – Earth Observing Laboratory, 1992–present: NCAR Integrated Sounding System (ISS). https://doi.org/10.5065/D6348HF9.

NSF NCAR – Earth Observing Laboratory, 2022: SWEX ISS Radiosonde Data - Sedgwick Site. Version 1.0. NCAR - Earth Observing Laboratory. https://doi.org/10.26023/H5TV-Y54J-R010.





Accepted for publication in *Weather and Forecasting*. DOI 10.1175/WAF-D-24-0084.1.

Parsons, D., and Coauthors, 1994: The integrated sounding system: Description and preliminary observations from TOGA COARE. *B. Am. Meteorol. Soc.*, **75 (4)**, 553–568.

Peltier, W., and T. Clark, 1979: The evolution and stability of finite-amplitude mountain waves. Part II: Surface wave drag and severe downslope windstorms. *J. Atmos. Sci.*, **36 (8)**, 1498–1529.

Rowson, D. R., and S. J. Colucci, 1992: Synoptic climatology of thermal low-pressure systems over south-western north America. *Int. J. Clim.*, **12 (6)**, 529–545.

Ryan, G., 1996: Downslope winds of Santa Barbara, California.

Sheridan, P., and S. Vosper, 2006: A flow regime diagram for forecasting lee waves, rotors and downslope winds. *Meteorol. Appl.*, **13 (2)**, 179–195.

Skamarock, W. C., and J. B. Klemp, 2008: A time-split nonhydrostatic atmospheric model for weather research and forecasting applications. *J. Comput. Phys.*, **227 (7)**, 3465–3485.

Smith, C., B. Hatchett, and M. Kaplan, 2018: Characteristics of Sundowner Winds Near Santa Barbara, CA, From a Dynamically Downscaled Climatology: Environment and Effects Aloft and Offshore. *J. Geophys. Res.-Atmos.*, **123 (23)**, 13 092–13 110.

Smith, R. B., 2018: 100 Years of Progress on Mountain Meteorology Research. *Meteorological Monographs*, **59**, 20–1.

Sukup, S., 2013: Extreme Northeasterly Wind Events in the Hills Above Montecito, California. *Western Region Technical Attachment NWS WR-1302. National Weather Service Western Region, Salt Lake City, UT*.

Tollinger, M., A. Gohm, and M. O. Jonassen, 2019: Unravelling the March 1972 northwest Greenland windstorm with high-resolution numerical simulations. *Q. J. Roy. Meteor. Soc.*, **145 (725)**, 3409–3431.

Tomine, K., 1984: A numerical study on local depressions on the lee side of the Hidaka mountain range in Hokkaido. *Journal of the Meteorological Society of Japan. Ser. II*, **62 (2)**, 215–223.

Wilks, D. S., 2011: *Statistical methods in the atmospheric sciences*, Vol. 100. Academic press, 676 pp pp.





Accepted for publication in *Weather and Forecasting*. DOI 10.1175/WAF-D-24-0084.1.

Zigner, K., L. Carvalho, S. Peterson, F. Fujioka, G.-J. Duine, C. Jones, D. Roberts, and M. Moritz, 2020: Evaluating the Ability of FARSITE to Simulate Wildfires Influenced by Extreme, Downslope Winds in Santa Barbara, California. *Fire*, **3 (3)**, 29.

Zigner, K., L. M. Carvalho, C. Jones, and G.-J. Duine, 2021: Extreme Winds and Fire Weather in Coastal Santa Barbara County, CA: An Observational Analysis. *Int. J. Clim.*, 1–22, https://doi.org/10.1002/joc.7262.

Zigner, K., and Coauthors, 2022: Wildfire Risk in the Complex Terrain of the Santa Barbara Wildland–Urban Interface during Extreme Winds. *Fire*, **5 (5)**, 138.





Accepted for publication in *Weather and Forecasting*. DOI 10.1175/WAF-D-24-0084.1.